ORIGINAL PAPER

AC conductivity and dielectric studies in polypyrrole wrapped tungsten disulphide composites

A. Sunilkumar[1] · S. Manjunatha[1,2] · Y. T. Ravikiran[3] · M. Revanasiddappa[4] · M. Prashantkumar[5] · T. Machappa[1]

Abstract

Using in situ chemical polymerization method, polypyrrole/tungsten disulphide (PPy/WS$_2$) composites were synthesized in various compositions viz. 10, 20, 30, and 40 wt% of WS$_2$ in polypyrrole. Composites were structurally and morphologically characterized by X-ray diffraction, Fourier transform infrared spectroscopy, Raman spectra, field emission scanning electron microscopy, energy-dispersive X-ray spectroscopy, transmission electron microscopy techniques. AC response studies of the composites at room temperature were carried out in the frequency range 50 Hz–1 MHz. When compared with pristine PPy, the composites have exhibited enhanced conductivity and the same has been reflected in the complex plane impedance plots. This indicates that the conduction mechanism is due to the hopping of charge carriers. The loss tangent curves of the composites have been explained using Rezlescu model.

A. Sunilkumar and S. Manjunatha of equal contribution.

✉ Y. T. Ravikiran
  ytrcta@gmail.com

✉ T. Machappa
  machappat@rediffmail.com

1 Department of Physics, VTURC, Ballari Institute of Technology and Management, Karnataka 583104, India

2 Department of Physics, V.V. Sangha's Independent P.U. College, Ballari, Karnataka 583104, India

3 Department of PG Studies in Physics, Government Science College, Chitradurga, Karnataka 577501, India

4 Department of Chemistry, PES University, Electronic City Campus, Bengaluru 560100, India

5 Department of Physics, Government College (Autonomous), Kalaburagi, Karnataka 585105, India

Introduction

Over the last quarter century, conducting polymers have turned out to be significant materials due to their wide range of technological applications viz., electronic devices [1], rechargeable batteries, sensors [2–4], drug delivery [5], conductive paints, super capacitors [6], and light-emitting devices [7]. These polymers possess alternating single and double bonds with π-conjugated polymer chains, which in turn has gifted the special electrical properties [8]. One of the major drawbacks of conducting polymers is their poor mechanical strength which can be overcome by filling the polymer matrix with metal/metal oxides and metalloids through chemical, electrochemical and mechanical mixing routes [9]. Conducting polymers like polypyrrole, polyaniline, polythiophene, and polyacetylene have got overwhelmed considerations in many fields [10]. Among them, polypyrrole and polyaniline polymers have emerged as outstanding materials due to their special transport properties, good environmental stability and facile synthesis. Polypyrrole and polyaniline composites of $PbTiO_3$ [11], SnO_2 [12], $MgFe_2O_4$ [13], Y_2O_3 [14], Nb_2O_5 [15], ZnO [16], $ZnWO_4$ [17], $NaVO_3$ [18], Fe_2O_3 [19] have been studied for their AC electrical properties so as to explore their potential applications in vivid fields. Apart from these oxides, novel conducting polymer composites of carbon nanotubes [20], graphene [21], and graphene oxide [22] have also been studied in the recent years. However, the synthesis and studies on AC electrical properties of conducting polymer-based composites filled with transition metal dichalcogenides (TMDs) are limited. The TMDs such as MoS_2, WS_2, TaS_2 [23–27], and phosphorene [28] are generally inorganic 2D layered materials which have been reported to play outstanding role in the fields of energy storage, sensors and optoelectronics applications [28, 29]. In this perspective, to enhance the scope of such TMDs based conducting polymer composites, we have embarked to study AC transport studies of PPy/WS_2 composites over a wide range of frequency. Here, we have preferred PPy because of its ease of synthesis, good stability, economic viability, and tunable surface charge properties which coup for the best synergy with the filling material [27]. Since WS_2 being a well-known TMD and in one of our recent studies, WS_2 has exhibited interesting results in AC conductivity, dielectric properties and humidity sensing characteristics with the polyaniline [31, 32]. Encouraged by the interesting results of WS_2, in the present paper we report the synthesis, structural–morphological characterization studies, AC conductivity studies over a wide range of frequency in PPy/WS_2 novel composites.

Experimental

Materials

Pyrrole [C_4H_4NH (98% purity)], ammonium persulphate [$(NH_4)_2S_2O_8$] were procured from S.D. Fine Chemicals, Mumbai, India. WS_2 (99.8%) metal basis is purchased from Alfa Aesar.

Synthesis of polypyrrole/tungsten disulphide composites

PPy/WS_2 composites were synthesized using chemical polymerization method as illustrated in the schematic diagram (Fig. 1). To synthesize the composites; finely ground tungsten disulphide powder was added (10, 20, 30 and 40 wt%) to pyrrole (0.03 M) and amalgamated by using magnetic stirrer. To get PPy/WS_2 composites, ammonium persulphate (0.06 M) was added drop-wise while uniform stirring. The precipitated product was purified by acetone and distilled water. To remove the water content, it was kept in oven at 100 °C till the constant weight was achieved. For different wt% of WS_2, namely 10, 20, 30 and 40%, the samples have been designated as PPy/WS_2-10%, PPy/WS_2-20%, PPy/WS_2-30% and PPy/WS_2-40% respectively. Similar procedure was followed to prepare polypyrrole without adding tungsten disulphide to the above reaction.

Characterization

FESEM images were captured by using instrument FEI Nova Nano SEM 600 by placing WS_2 on carbon tape while PPy and PPy/WS_2-30% on aluminium foil. Energy-dispersive X-ray spectrum (EDX) was obtained using EDAX genesis apparatus, fitted to the FESEM device. Raman spectra were obtained by Horiba Jobin Yvon lab Ram HR 800 spectrometer at a power of 20 mw using argon laser (514.5 nm) in the range 200 – 2000 cm^{-1}. X-ray diffraction (XRD) patterns of WS_2, PPy, and PPy/WS_2-30% samples were obtained by using Bruker D8 advance X-ray diffractometer, scanned in the 2θ range 10—80° at the rate of 1.1°min^{-1} using copper Kα as X-ray source of wavelength 1.541 Å. Fourier-transform infrared (FTIR) spectra were obtained in the wavenumber range 450–4000 cm^{-1} using Frontier Perkin Elmer FTIR spectrometer with a resolution of 4 cm^{-1} and 16
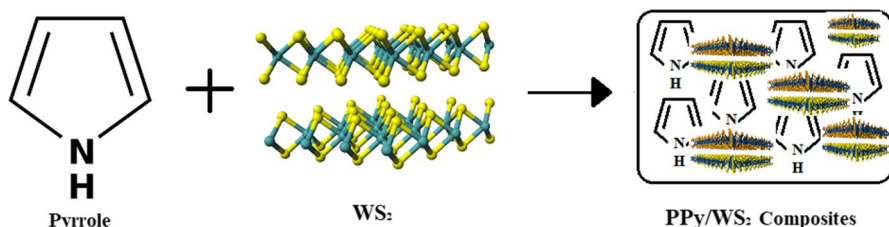

Fig. 1 Schematic representation of formation of PPy/WS_2 composites

scans. Transmission electron microscopy (TEM) image for PPy/WS$_2$-40% composite sample was captured using JEOL-3010 instrument.

AC conductivity and impedance measurements

At first, all the powder samples were grinded for two hours and then pressed under hydraulic pressure of 4 to 6 tons to form the pellets. Each pellet, having 10 mm diameter and 1 mm thickness was silver coated on either side of it, to get ohmic contacts. AC response parameters of each sample were recorded by a computer-controlled LCR metre (Hioki model 3532–50) with a frequency scale ranging from 50 to 1 MHz.
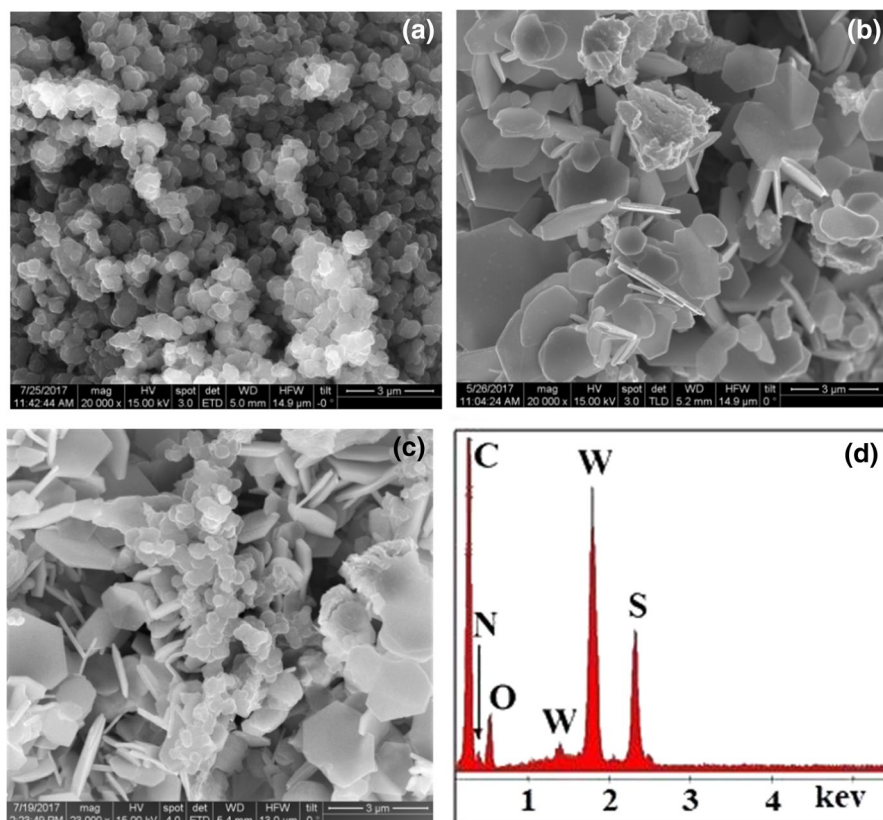

Fig. 2 FESEM images of **a** Polypyrrole, **b** WS$_2$, **c** PPy/WS$_2$-30% composite morphology, and **d** EDX spectrum of the composite

Results and discussion

FESEM and EDX studies

The as-prepared PPy/WS$_2$ composites have been subjected to FESEM to study the morphological properties of them. Figure 2 shows the morphology of PPy, WS$_2$, and PPy/WS$_2$-30% composite. Figure 2a depicts the FESEM image of pure polypyrrole revealing its granular morphology. It can be noted that the granules are consistently distributed throughout the sample [33]. Figure 2b shows 2D layered structure of WS$_2$ in the form of hexagonal sheets. These bundles of hexagonal sheets are having an area of few micrometres. Figure 2c shows the PPy/WS$_2$-30% composite wherein WS$_2$ hexagonal sheets are uniformly distributed in the PPy matrix. The incorporation of WS$_2$ into the PPy matrix has resulted in substantial morphological changes in the composite. As a result, chain orders in PPy have increased with the enhancement of electron delocalization of the composite evidencing increased conductivity. Figure 2d shows the EDX spectrum of PPy/WS$_2$ -30% composite confirming the presence of peaks related to the elements carbon, nitrogen and oxygen, which are the constituents of polypyrrole and the peaks related to tungsten and sulphur elements, which are the constituents of tungsten disulphide.

The distribution of grain size of PPy/WS$_2$-30% composite was studied using image J software and the related histogram is shown in Fig. 3. Histogram showing number of grains versus the grain size has revealed the average grain size in the composite, and it is found to be 2.6 µm.

Raman spectra

Figure 4 shows the Raman spectra of PPy, WS$_2$, and PPy/WS$_2$-30% composite. Figure 4a depicts the PPy manifested peaks at 1360 cm^{-1} which represent anti-symmetrical C–N$^{\bullet+}$ stretching in PPy and 1572 cm^{-1} represent C=C stretching vibrations of PPy backbone chains [34]. Figure 4b shows the Raman spectrum of WS$_2$ which has exhibited its signature peaks at 356 cm^{-1} owing to in-plane
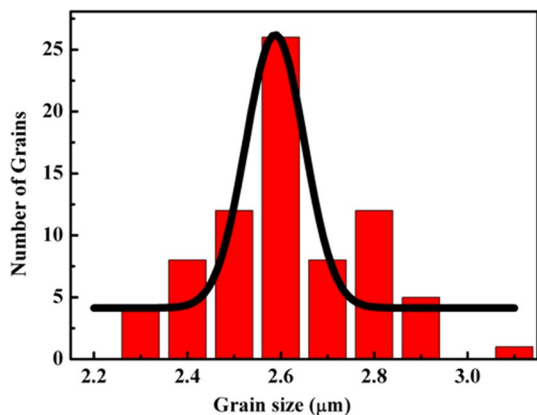

Fig. 3 Grain size distribution in PPy/WS$_2$-30% composite

Fig. 4 Raman spectra of **a** Polypyrrole, **b** WS$_2$, and **c** PPy/WS$_2$-30% composite
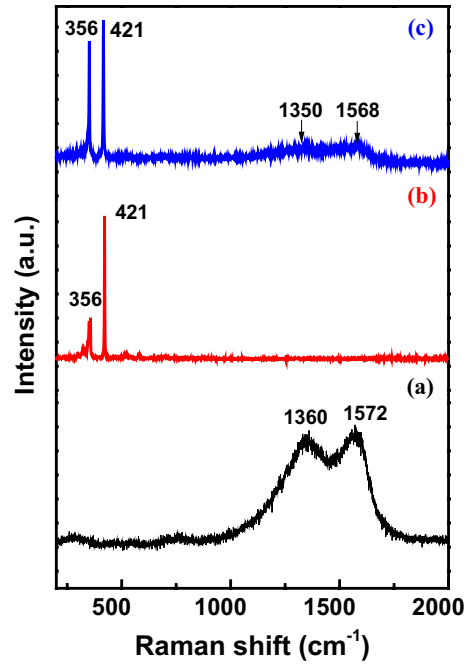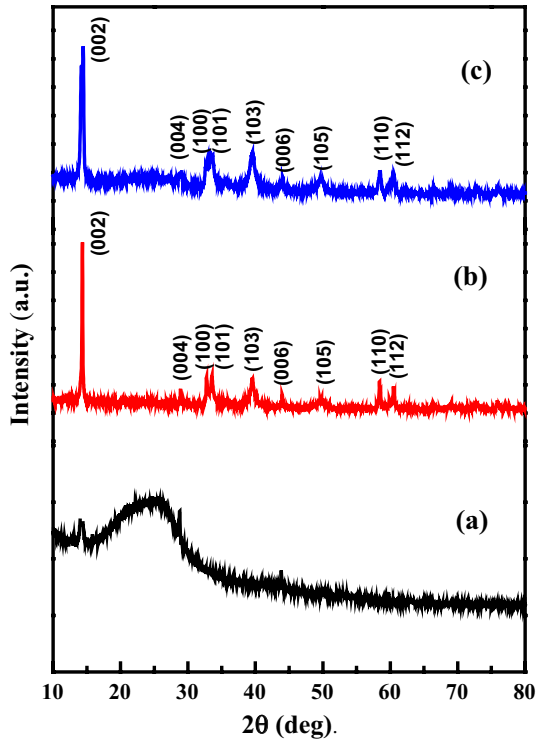
Fig. 5 XRD spectra of **a** Polypyrrole, **b** WS$_2$, and **c** PPy/WS$_2$-30% composite

phonon mode E_{2g}^1 and 421 cm^{-1} peak corresponding to out-of-plane phonon mode A_{1g}. Figure 4c of PPy/WS$_2$-30% composite shows the peaks at 356 and 421 cm^{-1} related to WS$_2$ and the broad bands of PPy have been suppressed in the composite due to the crystalline nature of WS$_2$ as revealed in XRD and SAED pattern of TEM image [35].

XRD studies

Figure 5 shows the X-ray diffraction studies of PPy, WS$_2$ and PPy/WS$_2$-30% composite. Figure 5a of PPy shows a broad diffraction peak around Bragg angle 25.77˚, exhibiting its amorphous nature. Figure 5b of WS$_2$ with designated (hkl) values evidence it's important peaks at Bragg angles 14.4˚, 28.9˚, 32.7˚, 33.5˚, 39.5˚, 44˚, 49.7˚, 58.4˚, and 60.5˚ with respect to their interplanar spacing distances; 6.18, 3.08, 2.73, 2.66, 2.27, 2.06, 1.83, 1.57, 1.52 Å respectively. Obtained data have been confirmed using standard JCPDS file No-08–237 [36]. Figure 5c of PPy/WS$_2$-30% composite reveals the pronounced peaks of WS$_2$ and the negligible peak of PPy in the composite, revealing its crystalline nature. The broad peak of PPy is vanished and is negligible due to the predominance of crystalline WS$_2$ in the composite, supporting the PPy wrapped WS$_2$. Similar structure has been observed in polyaniline/WS$_2$ composite in our earlier study [31].


Fig. 6 FTIR spectra of **a** Polypyrrole, **b** WS$_2$, and **c** PPy/WS$_2$-30% sample
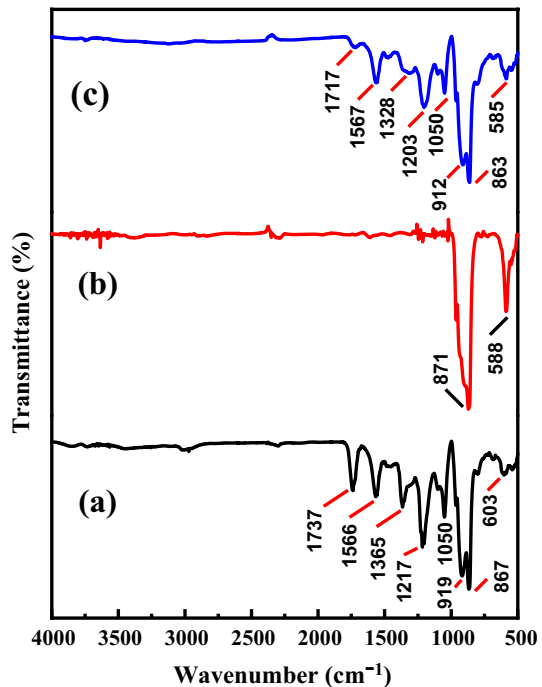
FTIR studies

Figure 6 shows the FTIR spectra of PPy, WS_2, and PPy/WS_2-30% composite. Figure 6a depicts FTIR spectrum of PPy showing its significant bands at 603, 867, and 919 cm^{-1} related to C-H wagging. The bands at 1050 cm^{-1} related to =C-H deformation, band at 1217 cm^{-1} correspond to C-N stretching vibrations, bands at 1365 and 1566 cm^{-1} corresponds to C-H in-plane stretching and ring stretching modes, respectively, and also the band at 1737 cm^{-1} is attributed to the C-N stretching all confirm the signature peaks of PPy. [37]. Figure 6b depicts the FTIR spectrum of WS_2 with the absorption bands at 588 and 871 cm^{-1} representing W-S stretching and S–S stretching vibrations, respectively [31]. FTIR spectrum of PPy/WS_2-30% composite has manifested the absorption bands of both WS_2 and PPy with small shifts validating the interaction between WS_2 and PPy due to the synergistic effects. The significant bands at 1717, 1328, 1203, 912, and 585 cm^{-1} in the composite corresponding to 1737, 1365, 1217, 919 and 603 cm^{-1} of PPy, respectively, all have been downshifted due to the chemical interaction between the active sites of PPy and WS_2 leading to the change in polymer conformation. Interestingly, the charge delocalization band of PPy at 1217 cm^{-1} has appeared in the composite at 1203 cm^{-1} with increased intensity indicating more conductive mature of the composite [38].

Fig. 7 **a** TEM image of PPy/WS_2-30% composite, **b** selected area electron diffraction captured on the darken regions of the composite
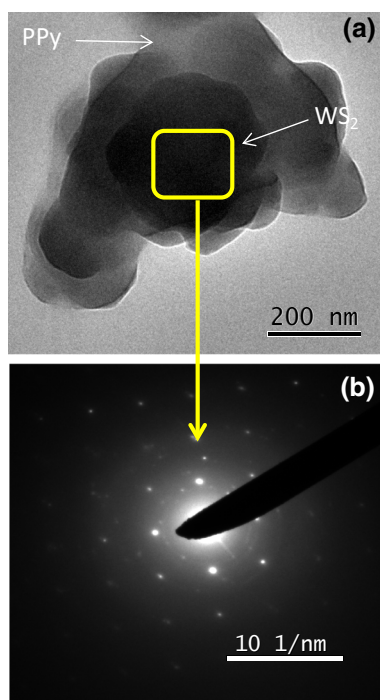
TEM analysis

Figure 7 shows the TEM image and SAED pattern of PPy/WS$_2$-30% composite. In Fig. 7a, the darker portion of the image represents WS$_2$, and the lighter region represents PPy, which is an indicative of formation of PPy epitomized WS$_2$ sheets. This has also been observed in terms of FESEM results as discussed in Sect. 3.1. Similar kind of epitomized conducting polymers of vivid filling materials are reported in the literature [39]. Figure 7b shows selected area electron diffraction pattern of the PPy/WS$_2$-30% composite. The bright spots in the pattern reveal the crystalline nature of the composite as evidenced from the XRD studies.

Impedance spectroscopy

The complex plane impedance plots of PPy and PPy/WS$_2$ composites are depicted in Fig. 8. Cole–Cole plots of all the samples manifests a deprived semicircle indicating the type of conduction mechanism involved in the composite system [40]. Here, the area under each curve was found to be decreasing with increasing wt% of WS$_2$ in PPy matrix, as seen in Fig. 8a. The area under Cole–Cole plot of PPy was observed to be much larger than the composites indicating its least conductivity which can be seen in Fig. 8b. PPy has exhibited a semicircle with lower conductivity which is the reminiscent of simple Debye-type relaxation mechanism. However, the composites show a moderate deviation from the perfect semicircle. These composites are considered to exhibit nearly Debye-type relaxation. The relaxation time for PPy and the composites were calculated using Eq. 1. Relaxation time for PPy was found to be 3.9 µs; however, for all the composites, it is found to be less than PPy, with a relaxation time range 0.15—0.39 µs as depicted in Table 1.

Relaxation time (τ),

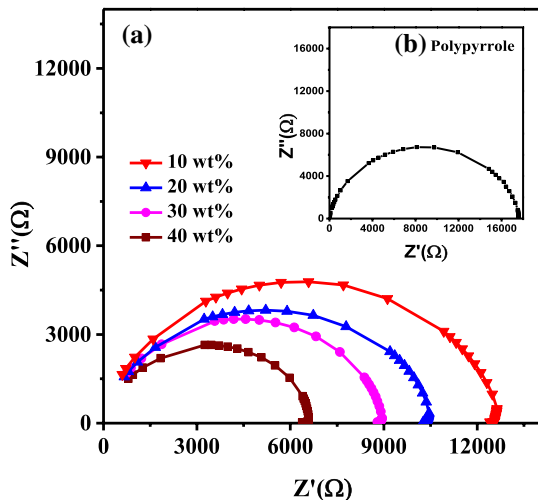Fig. 8 Cole–Cole impedance plots for **a** PPy/WS$_2$ composites, **b** PPy

Table 1 AC response behaviour of PPy/WS$_2$ composites

Sample	AC conductivity at 10 kHz (σ' S cm^{-1})	Power-law index (s)	Critical frequency (f_c kHz)	Relaxation time (τ µs)	Frequency at the relaxation peaks (f_p Hz)	Dielectric loss at 100 Hz (tan δ)
Polypyrrole	9.785×10^{-4}	0.20	200	3.91	4×10^4	21
PPy/WS$_2$-10%	1.850×10^{-3}	0.19	200	0.39	4×10^5	874
PPy/WS$_2$-20%	2.201×10^{-3}	0.20	100	0.31	5×10^5	897
PPy/WS$_2$-30%	2.831×10^{-3}	0.22	80	0.22	7×10^5	942
PPy/WS$_2$-40%	5.081×10^{-3}	0.26	50	0.15	1 X 10^6	1025

Fig. 9 Nyquist plots for PPy and PPy/WS$_2$ composites
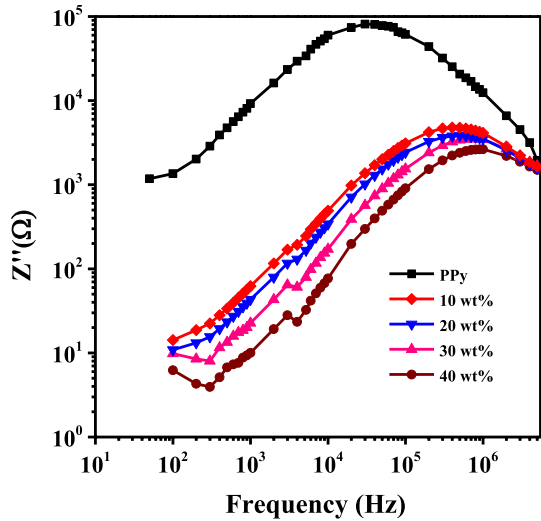
$$\tau = \frac{1}{2\pi f_p},\tag{1}$$

here f_p is the frequency corresponding to the peak point of Cole–Cole curve and it is also termed as relaxation frequency which is given in Table 1 for all the samples.

Nyquist plots of PPy and the composites were plotted as shown in Fig. 9. Variation of imaginary part of impedance with the applied AC frequency reveals compelling relaxation of the systems [41]. These traditional Nyquist plots show a single peak, specifying unique relaxation in the materials. Here, the peak position shifts from lower frequency to higher frequencies as the wt% of WS$_2$ is increased in

Fig. 10 Real part of AC conductivity versus applied frequency for PPy and its composites with 10, 20, 30 and 40 wt% of WS$_2$
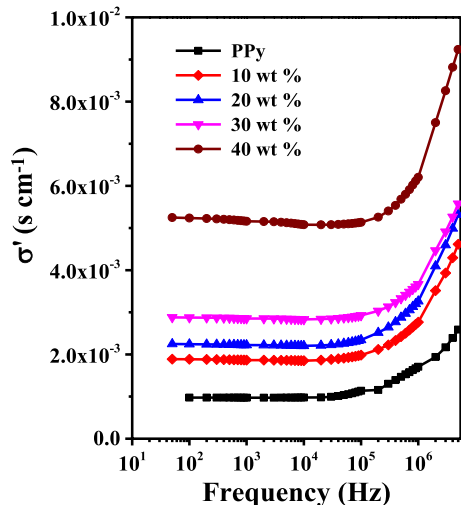
polypyrrole. The highest frequency can be observed for 40 wt% composite with fastest relaxation time of 0.15 μs. Lower value of relaxation time indicates decrease in hopping length of charge carriers and hence an increase in conductivity [42].
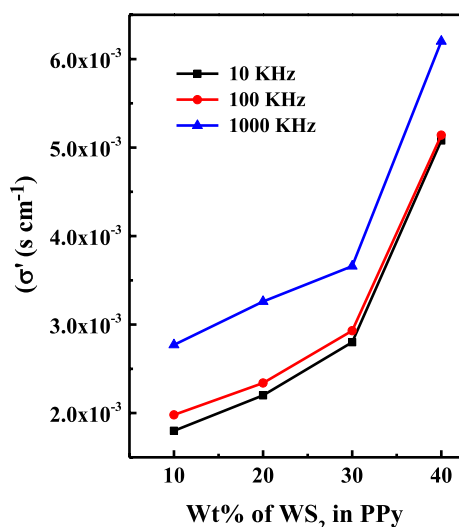
AC conductivity

AC conductivity for PPy and the composites were calculated using the equation as reported in our earlier papers [31, 43]. Figure 10 shows the frequency dependence of AC conductivity of PPy and the PPy/WS$_2$ composites. Initially, the conductivity was found to be consistent up to critical frequency. Above the critical frequency (f_c), conductivity was found varying linearly with increasing frequency which is in accordance with power law [44],

$$\sigma'(f) \propto f^s, \quad \text{when } f \, > \, f_c \tag{2}$$

From the above figure, it is clear that conductivity of the composites increase with increase in wt% of WS$_2$ in the matrix of PPy [45]. Incorporation of WS$_2$ in the matrix of PPy might have favoured the charge carriers to polarize at the suitable localized sites in the embedded structure of the composite as revealed in TEM, leading to the enhanced electrical conductivity. The conductivity pertaining to 10, 20, 30, and 40 wt% of the composite was observed to increase and for 40wt% composite, conductivity is maximum which is of nearly one order compared to the pristine PPy. However, for 50 wt% composite which is not shown in the figure, conductivity was found to decrease which may be ascribed to the increase in disorderliness in PPy chains and reduction in favourable localized sites due to the conformational changes in the PPy matrix [31].

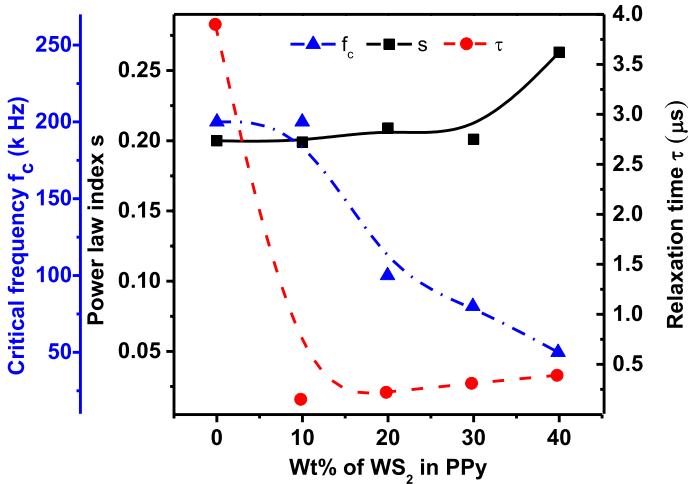**Fig. 11** Real part of AC conductivity versus wt% of WS$_2$ in PPy

Fig. 12 AC response changes in critical frequency, power-law index, and relaxation time with wt% of WS$_2$ in PPy composites

AC conductivity dependence on wt% of WS$_2$ in PPy composites is depicted in Fig. 11. Conductivity values at different frequencies (10, 100, and 1000 kHz) were plotted with increase in wt% of WS$_2$. Conductivity was observed to increase with the wt% of WS$_2$ in the composites. For 10, 20 and 30 wt% composites, the conductivity values were found to increase linearly till 30 wt%. However, for 40 wt% sample, the conductivity was found to increase enormously as depicted in Fig. 11. AC conductivities of all the samples at 10 kHz are shown in Table 1. Also, by considering least square fitting method for the conductivity values above the critical frequency, power-law index was calculated. The value obtained is an exponent mentioned in the power law as in Eq. 2. The index values (s) for the present samples lie in between 0.19 and 0.26 given in Table 1. From Fig. 12, we can see the behaviour of power-law index s, critical frequency f_c and relaxation time τ with respect to the wt% of WS$_2$ in the composite. The value of critical frequency has been found to decrease with increase in wt% of WS$_2$ in PPy. Among different composites, 40 wt% composite exhibited high conductivity and a less relaxation time. In general, as the conductivity of the composites increases, the relaxation time decreases and the same has been given in Table 1.

Dielectric loss

Figure 13 shows the frequency dependence of dielectric loss tangent of PPy and the composites. All the samples exhibited dielectric relaxation peak in the applied frequency range and these peaks are well described by using Rezlescu model, wherein the origin of relaxation peaks can be attributed to the total charge contribution both due to the p-type and n-type charge carriers [43]. Formation of dielectric loss peaks could also be realized based on polarons in the solid materials containing a narrow conduction band. Development of these polarons in the composite lead to the charge

Fig. 13 Loss tangent peaks for PPy and PPy/WS$_2$ composites
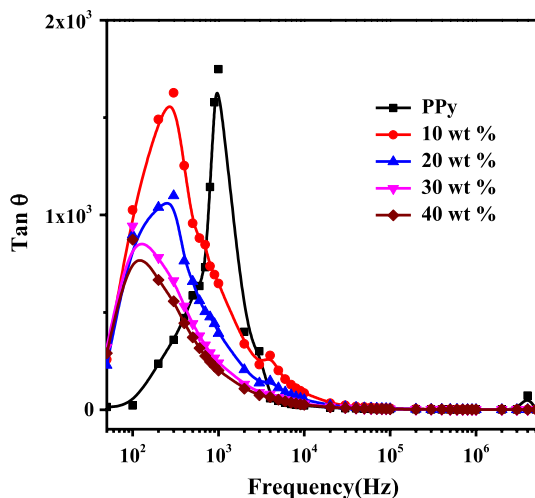
polarization. The relaxation peak is due to the relaxation loss at the resonant frequency between the applied AC field and the frequency of the hopping charge carriers. At 100 Hz, PPy exhibited dielectric loss tangent value of 21, whereas 10, 20, 30, and 40 wt% composites have shown dielectric loss tangent values of 874, 897, 942, and 1025 respectively. It is observed that with the increase in wt% of WS$_2$ in the composite the relaxation peak position has also been found to increase as given in Table 1. The highest dielectric loss at low frequencies can be explored for their potential applications in the fabrication of medium frequency devices.

Conclusion

A set of PPy/WS$_2$ based novel composites have been synthesized using in situ chemical polymerization technique. The morphological properties of pristine PPy and the PPy/WS$_2$ composites have been studied by FESEM technique. The room temperature AC conductivity and dielectric properties of the composites over a wide range of frequency has been investigated. Interestingly, PPy/WS$_2$-40% sample has exhibited highest conductivity among all the samples. The decrease in conductivity beyond 40 wt% of WS$_2$ may be attributed to the disorderliness of PPy matrix. AC conductivity in the composites is ascribed to the hopping of charge carriers and the frequency response behaviour has been explained using power law applicable to the disordered materials. Impedance studies through Cole–Cole and Nyquist plots suggest that the conductivity is electronic in nature. The dielectric behaviour has been understood by using Rezlescu model. These results suggest that the PPy/WS$_2$ composites have the potential to find applications in the design of medium frequency devices and the related fields. In conclusion, conducting polymer composites with TMDs form a novel class of hybrid materials providing huge opportunities to explore their potential applications in the fields of low-to-medium frequency devices, humidity, and gas sensors.

References

1. Xie D, Zhang M, Cheng F, BoFan H, Xie S, Liu P, Tu J (2018) Hierarchical MoS_2@ polypyrrole core–shell microspheres with enhanced electrochemical performances for lithium storage. Electrochim Acta 269:632–639

2. Sun A, Li Z, Wei T, Li Y, Cui P (2009) Chemical highly sensitive humidity sensor at low humidity based on the quaternized polypyrrole composite film. Sensors Actuators B Chem 142:197–203. https://doi.org/10.1016/j.snb.2009.08.028

3. Chethan B, Prakash HGR, Ravikiran YT, Kumari SCV, Manjunatha S, Thomas S (2020) Humidity sensing performance of hybrid nanorods of polyaniline-Yttrium oxide composite prepared by mechanical mixing method. Talanta 215:120906. https://doi.org/10.1016/j.talanta.2020.120906

4. Sunilkumar A, Manjunatha S, Machappa T, Chethan B, Ravikiran YT (2019) A tungsten disulphide–polypyrrole composite-based humidity sensor at room temperature. Bull Mater Sci 42:271. https://doi.org/10.1007/s12034-019-1955-5

5. Das TK, Prusty S (2012) Review on conducting polymers and their applications. Polym Plast Technol Eng 51:1487–1500. https://doi.org/10.1080/03602559.2012.710697

6. Tu CC, Peng PW, Lin LY (2018) Weight ratio effects on morphology and electrocapacitative performance for MoS_2/polypyrrole electrodes. Appl Surf Sci 444:789–799

7. Tessler N, Denton GJ, Friend RH (1996) Lasing from conjugated-polymer microcavities. Nature 382:695–697

8. Manjunatha S, Machappa T, Ravikiran YT, Chethan B, Sunilkumar A (2019) Polyaniline based stable humidity sensor operable at room temperature. Phys B Phys Condens Matter 561:170–178. https://doi.org/10.1016/j.physb.2019.02.063

9. Ćirić-Marjanovic G (2013) Recent advances in polyaniline composites with metals, metalloids and nonmetals. Synth Met 170:31–56. https://doi.org/10.1016/j.synthmet.2013.02.028

10. L.Y. H. Liu, J. Ge, E. Ma, Advanced biomaterials for biosensor and the ranostics, Elsevier Inc. (2019). doi:https://doi.org/10.1016/B978-0-12-813477-1.00010-4.

11. Stejskal J, Acharya U, Bober P, Hajná M, Trchová M, Mi M, Omastová M, Pa I, Gavrilov N (2019) Applied Surface Science Surface modification of tungsten disulfide with polypyrrole for enhancement of the conductivity and its impact on hydrogen evolution reaction. Appl Surf Sci 492:497–503. https://doi.org/10.1016/j.apsusc.2019.06.175

12. Acharya U, Bober P, Trchová M, Zhigunov A, Stejskal J (2018) Jiri Pfleger, Synergistic conductivity increase in polypyrrole/molybdenum disulfide composite. Polymer (Guildf) 150:130–137

13. Basavaraja C, Choi YM, Park HT, Huh DS, Lee JW, Revanasiddappa M, Raghavendra SC, Khasim S, Vishnuvardhan TK (2007) Preparation, characterization and low frequency AC conduction of polypyrrole-lead titanate composites. Bull Korean Chem Soc 28:1104–1108

14. Geng L, Zhao Y, Huang X, Wang S, Zhang S, Wu S (2007) Characterization and gas sensitivity study of polyaniline/SnO_2 hybrid material prepared by hydrothermal route. Sensors And Actuators B Chem 120:568–572

15. Megha R, Kotresh S, Ravikiran YT, Ramana CHVV, Kumari SCV, Thomas S (2017) Study of alternating current conduction mechanism in polypyrrole-magnesium ferrite hybrid nanocomposite through correlated barrier hopping model. Compos Interfaces 24:55–68. https://doi.org/10.1080/09276440.2016.1185298

16. T.K. Vishnuvardhan, V.R. Kulkarni, C. Basavaraja, S.C. Raghavendra, Synthesis , characterization and AC conductivity of polypyrrole / Y $_2$O $_3$ composites, 29 (2006) 77–83.

17. Ravikiran YT, Lagare MT, Sairam M, Mallikarjuna NN, Sreedhar B, Manohar S, MacDiarmid AG, Aminabhavi TM (2006) Synthesis, characterization and low frequency AC conduction of polyaniline/niobium pentoxide composites. Synth Met 156:1139–1147. https://doi.org/10.1016/j.synthmet.2006.08.005

18. Chougule MA, Dalavi DS, Patil PS, Moholkar AV, Agawane GL, Kim JH, Sen S, Patil VB (2012) Novel method for fabrication of room temperature polypyrrole – ZnO nanocomposite NO_2 sensor. Measurement 45:1989–1996. https://doi.org/10.1016/j.measurement.2012.04.023

19. Machappa T, Prasad MVNA (2009) Low frequency AC conduction in polyaniline / Zinc tungstate (PANI / ZnWO 4) composites. Ferroelectrics 392:71–80. https://doi.org/10.1080/00150190903412523

20. Machappa T, Prasad MVNA (2009) AC conductivity and dielectric behavior of polyaniline / sodium metavenadate (PANI / NaVO3) composites. Phys B Phys Condens Matter 404:4168–4172. https://doi.org/10.1016/j.physb.2009.07.194

21. Suri K, Annapoorni S, Sarkar AK, Tandon RP (2002) Gas and humidity sensors based on iron oxide-polypyrrole nanocomposites. Sens Actuators 81:277–282

22. Kapralova VM, Sapurina IY, Sudar NT (2018) Variation in the conductivity of polyaniline nanotubes during their formation. Semiconductors 52:816–819

23. Rao CNR, Sood AK, Subrahmanyam KS, Govindaraj A (2009) Graphene: The new two-dimensional nanomaterial. Angew Chemie - Int Ed 48:7752–7777. https://doi.org/10.1002/anie.200901678

24. Geleta GS (2018) Zhen Zhao, Zhenxin Wang, A novel reduced graphene oxide/molybdenum disulfide/polyaniline nanocomposite-based electrochemical aptasensor for detection of aflatoxin B-1. Analyst 143:1644–1649

25. Z. Hualian, L. Xingbin, W. Feifei, H. Zhufeng, H. Han, Fan Xueying, J. Junyi, Vertically aligned , polypyrrole encapsulated MoS$_2$ / graphene composites for high-rate LIBs anode Vertically aligned , Ceram. Int. 44 (2018) 7611–7617. doi:https://doi.org/10.1016/j.ceramint.2018.01.180.

26. Manjunatha S, Rajesh S, Vishnoi P, Rao CNR (2017) Reaction with organic halides as a general method for the covalent functionalization of nanosheets of 2D chalcogenides and related materials. J Mater Res 32:2984–2992. https://doi.org/10.1557/jmr.2017.224

27. Sunilkumar A, Manjunatha S, Chethan B, Ravikiran YT, Machappa T (2019) Polypyrrole – Tantalum disulfide composite : An efficient material for fabrication of room temperature operable humidity sensor. Sensors Actuators A Phys 298:111593. https://doi.org/10.1016/j.sna.2019.111593

28. Vishnoi P, Rajesh S, Manjunatha S, Bandyopadhyay A, Barua M, Pati SK, Rao CNR (2017) Doping phosphorene with holes and electrons through molecular charge transfer. ChemPhysChem 18:2985–2989. https://doi.org/10.1002/cphc.201700798

29. Chao J, Yang L, Liu J, Hu R, Zhu M (2018) Sandwiched MoS$_2$/polyaniline nanosheets array vertically aligned on reduced graphene oxide for high performance supercapacitors. Electrochim Acta 270:387–394

30. Rao CNR, Gopalakrishnan K, Maitra U (2015) Comparative study of potential applications of graphene, MoS$_2$, and other two-dimensional materials in energy devices, sensors, and related areas. ACS Appl Mater Interfaces 7:7809–7832. https://doi.org/10.1021/am509096x

31. Manjunatha S, Machappa T, Sunilkumar A, Ravikiran YT (2018) Tungsten disulfide: an efficient material in enhancement of AC conductivity and dielectric properties of polyaniline. J Mater Sci Mater Electron 29:11581–11590. https://doi.org/10.1007/s10854-018-9255-1

32. Manjunatha S, Chethan B, Ravikiran YT, Machappa T (2018) Room temperature humidity sensor based on polyaniline- tungsten disulfide composite. AIP Conf Proc 1953:030096–1–030096–4. https://doi.org/10.1063/1.5032431

33. Tomšík E, Morávková Z, Stejskal J, Trchová M, Zemek J (2012) In situ polymerized polyaniline films: the top and the bottom. Synth Met 162:2401–2405

34. Li M, Wei Z, Jiang L (2008) Polypyrrole nanofiber arrays synthesized by a biphasic electrochemical strategy. J Mater Chem 18:2276–2280. https://doi.org/10.1039/b800289d

35. Crowley K, Cassidy J (2003) In situ resonance Raman spectroelectrochemistry of polypyrrole doped with dodecylbenzenesulfonate. Jourrnal Electroanal Chem 547:75–82. https://doi.org/10.1016/S0022-0728(03)00191-8

36. Chougule MA, Sen S, Patil VB (2011) Facile and efficient route for Microstructural, preparation of polypyrrole–ZnO nanocomposites: Properties, optical and charge transport. J Appl Polym Sci. https://doi.org/10.1002/app.36475

37. Chethan B, Prakash HGR, Ravikiran YT, Vijayakumari SC, Thomas S (2019) Polypyyrole based core-shell structured composite based humidity sensor operable at room temperature. Sensors Actuators B Chem. https://doi.org/10.1016/j.snb.2019.126639

38. Megha R, Ravikiran YT, Kumari SCV, Prakash HGR, Tiwari SK, Thomas S (2018) Enhancement in alternating current conductivity of polypyrrole by multi- walled carbon nanotubes via single electron tunneling. Diam Relat Mater 87:163–171

39. Manjunatha S, Machappa T, Ravikiran YT, Chethan B, Revanasiddappa M (2019) Room temperature humidity sensing performance of polyaniline – holmium oxide composite. Appl Phys A 125:361. https://doi.org/10.1007/s00339-019-2638-1

40. Badi N, Khasim S, Roy AS (2016) Micro-Raman spectroscopy and effective conductivity studies of graphene nanoplatelets/polyaniline composites. J Mater Sci Mater Electron 27:6249–6257. https://doi.org/10.1007/s10854-016-4556-8

41. Maity N, Kuila A, Das S, Mandal D, Shit A, Nandi AK (2015) Optoelectronic and photovoltaic properties of graphene quantum dot–polyaniline nanostructures. J Mater Chem A 3:20736–20748. https://doi.org/10.1039/C5TA06576C

42. I. Sadiq, S. Naseem, M. Naeem Ashiq, M.A. Khan, S. Niaz, M.U. Rana, Structural and dielectric properties of doped ferrite nanomaterials suitable for microwave and biomedical applications, Prog. Nat. Sci. Mater. Int. 25 (2015) 419–424. doi:https://doi.org/10.1016/j.pnsc.2015.09.011.

43. Manjunatha S, Sunilkumar A, Ravikiran YT, Machappa T (2019) Effect of holmium oxide on impedance and dielectric behavior of polyaniline–holmium oxide composites. J Mater Sci Mater Electron 30:10332–10341. https://doi.org/10.1007/s10854-019-01371-4

44. Bisquert J, Belmonte GG (2004) Interpretation of AC conductivity of lightly doped conducting polymers in terms of hopping conduction. Russ J Electrochem 40:352–358

45. Xu BH, Lin BZ, Chen ZJ, Li XL, Wang QQ (2009) Preparation and electrical conductivity of polypyrrole/WS_2 layered nanocomposites. J Colloid Interface Sci 330:220–226

⌐ Springer